IEEE Trans. Nucl Sci., vol. NS-45, pp. 1268–1272, 1998.

Calibration of a PET Detector Module that Measures Depth of Interaction*

J. S. Huber†, *Member, IEEE* , W.W. Moses†, *Senior Member, IEEE*, P. R. G. Virador†
†Lawrence Berkeley National Laboratory, University of California, Berkeley, CA 94720

Abstract

We have investigated two *in situ* calibration techniques (using gamma rays incident from the patient side) for PET detector modules that measure interaction depth via an analog ratio. We need to determine two unknowns: the gain ratio *K* of the two detector (PMT and PD) signals and the depth dependence α of the signals (defined as the ratio of the signal observed when the crystal is excited at the end closest to and furthest from the detector). The depth dependence is assumed to be linearly dependent on distance from the detector end, in agreement with experimental results. The first method extracts *K* and α using (a) the ratio of the PMT and PD signals for interactions that occur in the detector end closest to the patient (the most probable depth) and (b) the shape of the PMT pulse height distribution which reflects the exponential attenuation length in the detector. The second method utilizes the fact that E=PD+PMT (the total energy estimator) is independent of Γ=PD/(PD+PMT) (the depth estimator) when *K* is correct, with a distribution position that is α dependent. Simulations indicate that both the gain ratio and depth dependence can be determined with an error of 3% rms and 2% rms respectively, resulting in minimal degradation of energy and depth resolution.

I. Introduction

We have previously described the design for a PET detector module that consists of an array of LSO crystals coupled on one end to a photomultiplier tube and on the opposite end to an array of silicon photodiodes [1]. We have calibrated this prototype detector module using an electronically collimated beam of annihilation photons incident from the side of the detector to excite at a specified depth of interaction (figure 1a). Others have suggested calibrating different depth-encoding PET detectors using techniques similarly dependent on measurements with side incident beams to provide a photopeak pulse height versus depth look-up table [2-3]. However, using side incident gamma rays is awkward for complete cameras since recalibration is only possible by removing detectors from the gantry.

We therefore investigate *in situ* calibration techniques (*i.e.* those that utilize only gamma rays incident from the patient side of the detector module such as in figure 1b) using a Monte Carlo simulation that includes the measured electronic noise, energy resolution, and signal levels, as well as energy dependent Compton and photoelectric cross sections in LSO. The light collection is assumed to be linearly dependent on the distance of interaction from the photodetector, which has been empirically found to be a good approximation [1]. More precisely, the PD and PMT signals (in ADC counts) for an ideal detector are given as a function of depth *x* by:

$$PD(x) = \frac{E}{\alpha} k_{pd} \left[(\alpha - 1)\left(1 - \frac{x}{L}\right) + 1\right] \quad (1)$$

$$PMT(x) = \frac{E}{\alpha} k_{pmt} \left[(\alpha - 1)\frac{x}{L} + 1\right], \quad (2)$$

where k_{pd} and k_{pmt} are the gain factors that convert energy deposition to ADC counts for each photodetector, *E* is the energy deposit in the crystal, *L* is the crystal length, and α is the depth dependence (defined as the ratio of the signal observed when the crystal is excited at the end closest to and furthest from the photodetector). Depth *x* is defined to be 0 at the PD photodetector. Figure 2 shows these detector signals as

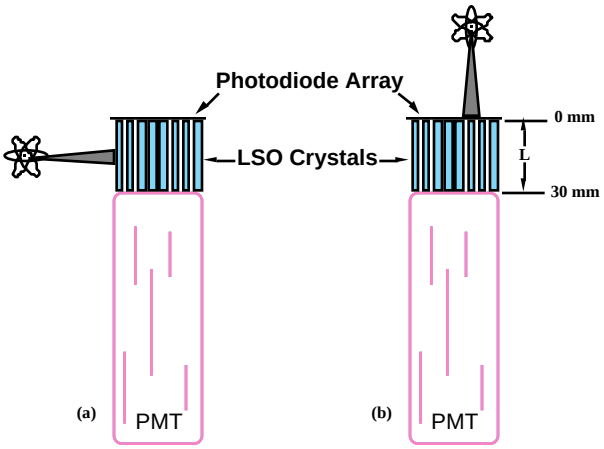

Figure 1: Calibration geometry for a depth of interaction detector module. An electronically collimated beam of annihilation photons are incident from (a) the side of the detector module to excite at a specified depth of interaction or (b) the patient side of the detector module for *in situ* calibration.

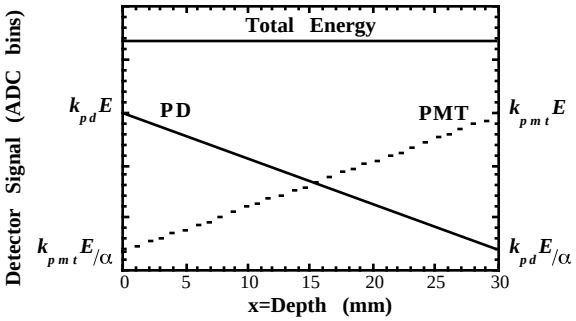

Figure 2: The PD and PMT detector signals, which are linearly dependent on the depth of interaction (*x*) from the photodetector. The depth *x* is defined to be 0 at the PD photodetector. Total energy is the sum of PD and PMT.

* This work was supported in part by the U.S. Department of Energy under Contract No. DE-AC03-76SF00098, in part by Public Health Service Grant Nos. P01-HL25840 and R01-CA67911, and in part by Breast Cancer Research Program of the University of California Grant No. 1RB-0068.

a function of depth for an ideal detector, assuming noise free readout, perfect energy resolution, and monoenergetic energy deposition.

The necessary calibration parameters are depth dependence (α) and the relative gain of the PMT and PD (K). More specifically,

$$\alpha = \frac{\mathrm{PMT}(x=L)}{\mathrm{PMT}(x=0)} = \frac{\mathrm{PD}(x=0)}{\mathrm{PD}(x=L)} \qquad (3)$$

$$K \equiv \frac{k_{pmt}}{k_{pd}} = \frac{\mathrm{PMT}(x=L)}{\mathrm{PD}(x=0)} = \alpha \frac{\mathrm{PMT}(x=0)}{\mathrm{PD}(x=0)}. \qquad (4)$$

In this paper we present two different *in situ* calibration methods used to extract K and α.

II. Simulation

Monte Carlo data is used to simulate the performance of a single LSO crystal coupled on one end to a silicon photodiode and on the opposite end to a photomultiplier tube. Normally incident 511 keV photons enter the crystal on the PD end and interact in the crystal via Compton scattering and/or photoelectric absorption, assuming energy dependent cross sections in LSO. A 1.2 cm attenuation length ($1/\mu$) of LSO is assumed [4]. Since there is only a single simulated crystal, Compton scattered photons that escape the crystal are lost.

The photodetectors are assumed to have a quantum efficiency of 0.8 and 0.2 for the PD and PMT, respectively. The detected signal is smeared by a Gaussian distribution to simulate the affect of finite scintillator energy resolution. The rms width of the Gaussian is proportional to the square-root of the signal and the proportionality constant is chosen to match observed energy resolution in LSO. This scintillator based "noise" is summed in quadrature with the measured electronic noise (190 electrons rms for PD and 0 for PMT detector). The signal in terms of energy is multiplied by the gain factor k_{pd} (or k_{pmt}) to give the signal PD (or PMT) in terms of ADC bins. Thus, the total energy resolution at 511 keV is ~19% fwhm with energy dependence; this is pessimistic compared to the expected detector performance [1] but represents a worst case scenario in terms of energy resolution. Calibration results extracted with a smaller proportionality constant were found not to affect the results. We want to extract the relative gain K and calibrate so that 1 PMT ADC bin equals 1 PD ADC bin after correction.

III. Exponential Attenuation Method

The light collection is linearly dependent on the depth, thus the exponential nature of annihilation photon interaction in the crystal is reflected in the exponential shape of the PMT and PD pulse height spectra. The first calibration method that we describe utilizes this exponential shape.

Figure 3 demonstrates the underlying data that is used for the calibration. Consider 511 keV gammas that interact only via photoelectric effect in a noise free detector. Interactions at a single depth would appear as a delta function in the pulse height distribution. As the distribution of interaction depths is exponential (due to exponential attenuation in LSO), the PD and PMT pulse height spectra also have exponential slopes. The PMT spectrum has a clear peak at low pulse height bins, corresponding to interactions at the patient end of the scintillation crystal ($x=0$, the most probable depth). Because of light sharing, interactions at $x=L$ (*i.e.* close to the PMT) populate high pulse height bins. Ideally, we could use the four edges of the spectra — PD($x=0$), PD($x=L$), PMT($x=0$) and PMT($x=L$) — to extract the calibration constants using equations (3) and (4).

For a realistic detector that includes electronic noise, finite energy resolution, and Compton scatter (as in figure 4), we can still identify the peaks corresponding to interactions at $x=0$. However, it becomes difficult to accurately identify the pulse height edges for the $x=L$ interactions. Thus, we have developed an algorithm to determine K and α using the $x=0$ peaks and the shape of the PMT spectrum.

For a realistic detector, Gaussian smearing of the PMT pulse height spectrum rounds off the abrupt edges seen at $x=0$ and $x=L$ in figure 3 and alters the exponential shape near these x values. However, the shape is unaffected for $0.1L \le x \le 0.9L$. Thus the PMT pulse height spectrum is fit with an exponential over a limited region — from 5% above the $x=0$ peak to 25% below the bin where the PMT spectrum tail first goes to zero — in order to extract the slope m ($N = N_0 \exp(-b-mPMT) = N_0 \exp(-x/\mu)$). The PMT($x=0$) peak is estimated by

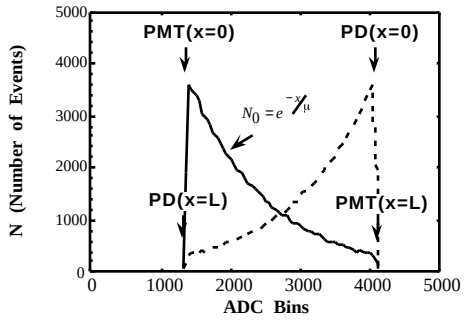

Figure 3: The PMT and PD distributions simulated with α=3 and K=1 for an ideal detector. Exponential attenuation ($1/\mu$) is evident for both PD and PMT distributions, as well as the edges corresponding to $x=0$ and $x=L$.

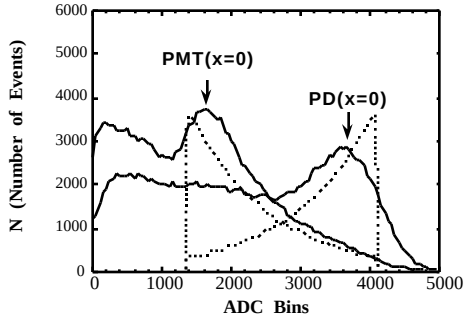

Figure 4: The PMT and PD distributions simulated with α=3 and K=1 for a realistic detector. Exponential attenuation ($1/\mu$) is evident for the PMT distribution (to the right of its peak), as well as the edges corresponding to $x=0$.

the ADC bin with the maximum number of events. The combination of the peak PMT($x=0$) and exponential slope m are used to extract alpha:

$$\alpha = 1 + \frac{L}{m\ \mu\ \mathrm{PMT}(x=0)}. \qquad (5)$$

The PD pulse height spectrum peaks for interactions corresponding to $x=0$, which is also estimated by the ADC bin with the maximum number of events. We can then obtain the relative gain factor K from PMT($x=0$) and PD($x=0$) using equation (4).

We need to correct for systematic errors, such as those caused by the PMT($x=0$) and PD($x=0$) peak finding algorithm (see figure 4). To obtain these correction factors, a data set of 20 runs was simulated with different (α,K) combinations and 200k events per run. The true (*i.e.* input) α and K constants ranged in value from 2–4 and 0.5–1.5 respectively to fully cover the expected detector conditions. The nominal values are α=3 and K=1. This calibration data set was used to measure "raw values" of α and K with the exponential attenuation method described above. We plot the measured raw versus true values and fit a line for both α and K, providing correction factors for future data sets.

To estimate the errors in this method, a second data set of 20 runs was simulated with 200k events each and the same (α,K) combinations as in the calibration data set but with different random seeds. The exponential attenuation method was applied to each run, then corrected with the corresponding α or K calibration line. Figure 5 shows the resulting measurements for α and K as a function of the true values. A line of slope 1 is also shown to represent the desired values. Thus, we obtain α with a 3% rms error and K with a 2% rms error using this method. In figure 6, the pulse height spectra and depth of interaction distributions are shown when using either the true or measured calibration constants. The calibration errors cause only a minimal degradation of the energy and depth resolution.

This technique uses only a crude estimation of the pulse height peaks (PMT($x=0$) and PD($x=0$)) by using the bin with the maximum number of events for each photodetector. Clearly a more sophisticated fit for the peak region would give a better estimation. In addition, the PMT spectrum should be fit with an exponential after the Compton background has been subtracted. However, our investigation showed accurate slope extraction when fitting without subtraction. For speed and simplicity, we choose not to fit the peaks or subtract off the background since they weren't necessary. A run of 200k events is a very large sample when considering that we have over 20000 crystals in need of calibration in our proposed PET camera. However, we believe that this technique or a minor variant will yield excellent results even with a smaller number of events.

IV. Constant Energy Sum Method

The second calibration method utilizes the fact that the total energy estimator (E=PD+PMT) is independent of the depth estimator (Γ=PD/(PD+PMT)) if the relative gain K is correct. Figure 2 shows the PD, PMT, and total energy detector signals as a function of true interaction depth for an ideal detector with a correct relative gain of 1. Figure 7 shows the total energy as a function of the depth estimator for an ideal detector with either K=1 (figure 7a) or K=1.5 (figure 7b).

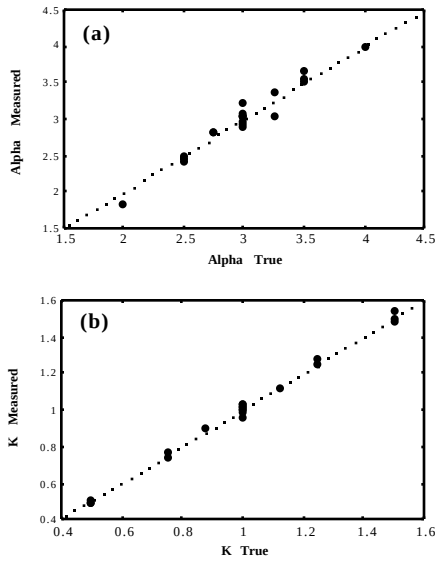

Figure 5: The correlation between true and measured calibration constants using the exponential attenuation method for (a) α and (b) K. The lines of slope 1 represent the desired values.

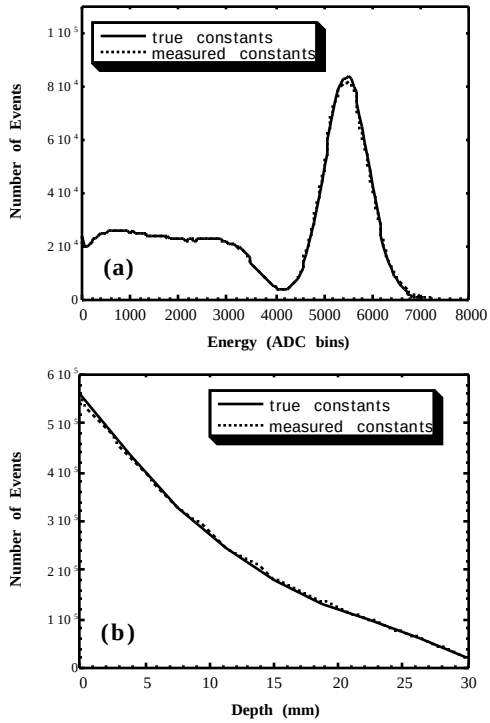

Figure 6: The (a) total energy pulse height spectrum and (b) depth of interaction distribution for both the true and measured calibration constants. The curves are almost indistinguishable, indicating minimal degradation in energy and depth resolution due to calibration using the exponential attenuation method.

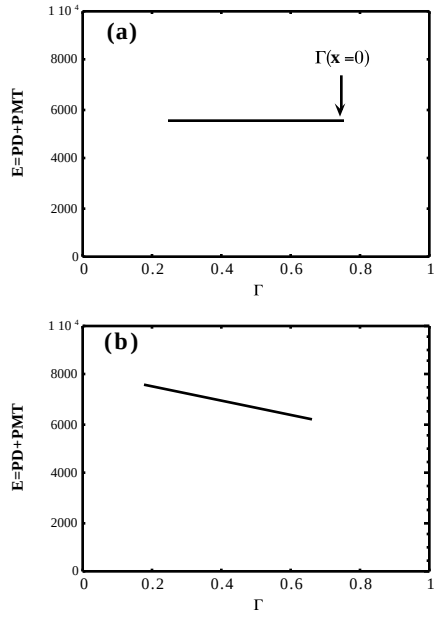

Figure 7: The total energy estimator E=PD+PMT as a function of the depth estimator Γ=PD/(PD+PMT) for an ideal detector with α=3 and (a) a correct relative gain of *K*=1 or (b) an incorrect gain of *K*=1.5. Total energy is independent of Γ if the gain is correct.

A clear dependence on Γ is observed when the gain is incorrect, whereas the total energy is flat when the gain is correct. Thus we can estimate *K* from the slope of E as a function of Γ. Figure 7 also shows that the total energy position is a function of the calibration constants; the line is centered for correct gain (figure 7a) and shifts to the left for *K*>1 (figure 7b). More precisely, the upper edge is given by

$$\Gamma(x=0) = \frac{\alpha}{\alpha + K}. \qquad (6)$$

Thus we can extract the calibration constant α by measuring the upper edge Γ(*x=0*) once we have determined *K*.

For a realistic detector that includes electronic noise, finite energy resolution and Compton scatter, the lines in figure 7 become a scatter plot of E verses Γ but still demonstrate independence of Γ if the gain is correct (figure 8). Figure 8 also shows an excellent separation between photopeak and Compton scatter events for both correct and incorrect gains. In order to properly extract *K* from the scatter plot for a realistic detector, we select only the photopeak events using an expectation maximization technique [5]. We model the probability densities of the events in the variables Γ and E as a mixture of two Gaussian functions and classify each event according to Bayesian inferencing [6]. The white line in figure 8b, corresponding to the average E as a function of Γ for photopeak events only, is a shifted hyperbola. Thus rather than fitting E, we make a linear fit of the inverse of E. We extract *K* from the slope and intercept of this line, giving an excellent fit for photopeak events as seen in figure 8. We are able to observe a clear upper edge Γ(*x=0*) for all *K* values. This edge is determined by histograming Γ and estimating the peak by the bin with the maximum number of events. We can then determine α from both *K* and Γ(*x=0*) using equation (6).

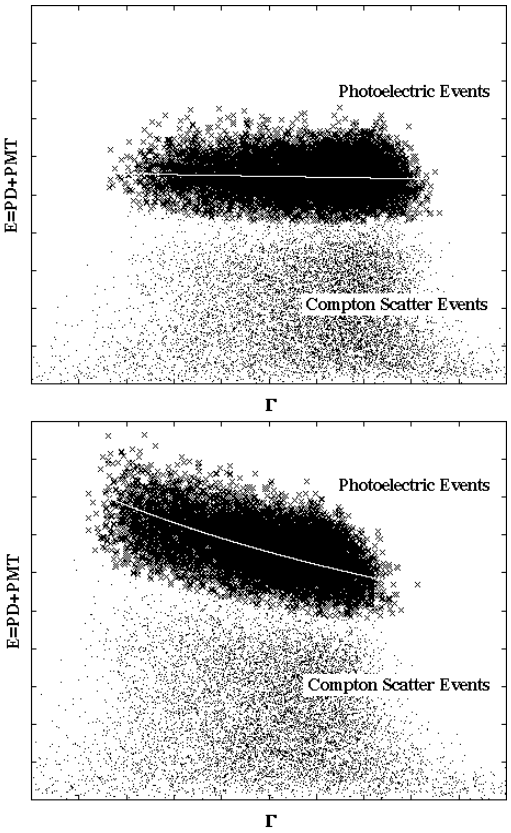

Figure 8: The total energy estimator E=PD+PMT as a function of the depth estimator Γ=PD/(PD+PMT) for a realistic detector with α=3 and (a) a correct relative gain of *K*=1 or (b) an incorrect gain of *K*=1.5. Total energy is independent of Γ if the gain is correct. The crosses indicate photoelectric events and the dots are Compton scatter events, as determined by an expectation maximization technique. The white lines are a fit of only photoelectric events (used to extract *K*).

The same calibration data set used to measure α and *K* with the exponential attenuation method (describedpreviously) was used for the constant energy sum method. However, only the first 20k events per run were used because of the computation time required by the expectation maximization algorithm. There are systematic errors such as the position of the Γ(*x=0*) peak, but the calibration results show a correlation between the measured raw values and the true values. We plot the measured raw versus true values and fit a line for both α and *K*, providing correction factors for future data sets.

In order to estimate the errors, the constant energy sum method was applied to the same test data set used for the exponential attenuation method but using only the first 20k events. These measured raw values of α and *K* were then corrected with the corresponding α or *K* calibration line. Figure 9 shows the resulting measurements for α and *K* as a function of the true values. Thus, we obtain α with a 14% rms error and *K* with a 4% rms error using this method. Although the rms error for α is much larger for this method when compared to the previous method (with 2% rms for α), the calibration errors cause only a minimal degradation of the energy and depth resolution (figure 10).

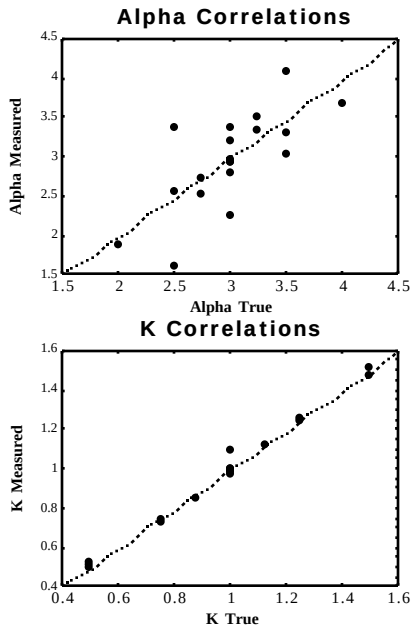

Figure 9: The correlation between true and measured calibration constants using the constant energy sum method for (a) α and (b) *K.* The lines of slope 1 represent the desired values.

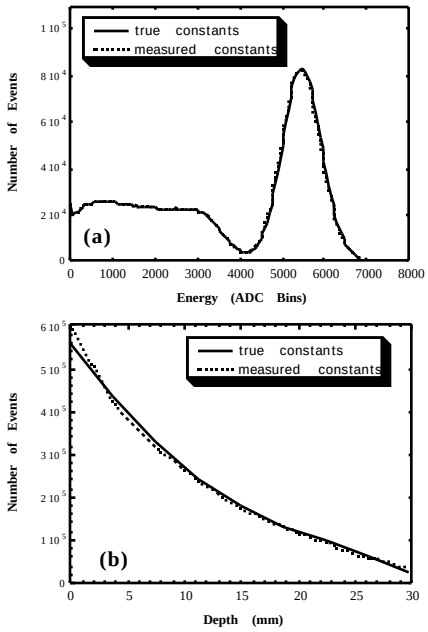

Figure 10: The (a) total energy pulse height spectrum and (b) depth of interaction distribution for both the true and measured calibration constants. Excellent agreement is seen, indicating minimal degradation in energy and depth resolution due to calibration using the constant energy sum method.

V. Conclusions

We have investigated two *in situ* calibration techniques for PET detector modules that measure depth via an analog ratio. The first method uses the ratio of the detector signals at the most probable depth as well as the exponential shape of the PMT pulse height spectrum in order to extract the calibration constants. We obtain the depth dependence (α) with a 3% rms error and the relative detector gain (*K*) with a 2% rms error using this exponential attenuation method. In the second method we select photopeak events and fit the total energy versus depth estimator (Γ) shape to extract *K*; we then determine α from both *K* and the upper edge Γ(*x=0).* We obtain the depth dependence with a 14% rms error and the relative detector gain with a 4% rms error using this constant energy sum method. The larger errors in the constant energy sum method may be due to the smaller number of events (20k vs. 200k). However, both calibration techniques cause only minimal degradation of the energy and depth resolution so they are both viable options for *in situ c*alibration. These methods depend on the ratio of two detectors to give depth information, but they can be applied to many types of detectors. One could also apply similar methods to designs using only one detector in order to calibrate or verify depth information.

VI. Acknowledgments

We wish to acknowledge the substantial contribution of Mr. Jonathan Maltz to the development of the constant energy sum method. This work was supported in part by the Director, Office of Energy Research, Office of Biological and Environmental Research, Medical Applications and Biophysical Research Division of the U.S. Department of Energy under contract No. DE-AC03-76SF00098, in part by the National Institutes of Health, National Heart, Lung, and Blood Institute, National Cancer Institute, and National Institute of Neurological Disorders and Stroke under grants No. P01-HL25840 and R01-CA67911, and in part by the Breast Cancer Fund of the State of California through the Breast Cancer Research Program of the University of California under grant No. 1RB-0068.

VI. References

[1] J.S. Huber, W.W. Moses, et al., "Characterization of a 64 Channel PET Detector Using Photodiodes for Crystal Identification," *IEEE Trans. Nucl. Sci.,* vol. NS-44, pp. 1197-1201, 1997.

[2] J.G. Rogers, C. Moisan, et al., "A Practical Block Detector for a Depth-Encoding PET Camera," *IEEE Trans. Nucl. Sci.*, vol. NS-43, pp. 3240-3248, 1996.

[3] J.L. Robar, C.J. Thompson, et al., "Construction and calibration of detectors for high-resolution metabolic breast cancer imaging," *Nucl. Instr. and Meth. in Phys. Res.*, vol. A 392, pp. 402-406, 1997.

[4] C.L. Melcher and J.S. Schweitzer, "Cerium-doped lutetium orthosilicate: A fast, efficient new scintillator," *IEEE Trans. Nucl. Sci.*, vol. NS-39, pp. 502, 1992.

[5] A.P. Dempster, N.M. Laird, et al., "Maximum Likelihood from Incomplete Data via the EM Algorithm," *Journal of the Royal Statistical Society*, B 39, pp. 1-38, 1977.

[6] C. Bishop, Neural Networks for Pattern Recognition, 1996, pp. 59-73.